# Supplemental Information for:

## Effects of porous guest sizes of magnetic porous liquids on lead ion adsorption from the aqueous solution

Ying Zhang,[a,b] Ruilu Yang,[a*] Jian Shi[a,b] and Jian Zhang[a]

a Analysis and Testing Center, Nantong University, Nantong 226019, China.

b School of Transportation and Civil Engineering, Nantong University, Nantong 226019, China.

Corresponding author: * Ruilu Yang, E-mail address: yangruilu1987@126.com

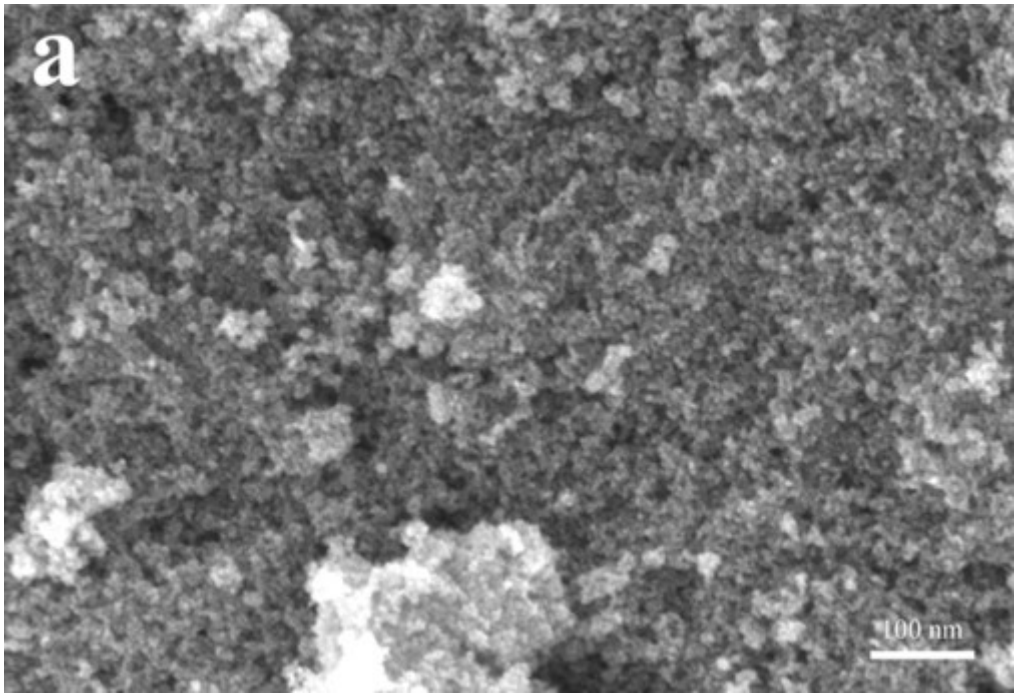


Fig. S1. The SEM images of $Fe_3O_4$ [75]

Fig. 1S shows the SEM image of $Fe_3O_4$ nanoparticles. The dark spots in the image correspond to the $Fe_3O_4$ nanoparticles. It can be observed that the $Fe_3O_4$ powder nanoparticles exhibit a pronounced aggregation phenomenon, overlapping with each other due to their relatively high surface energy.

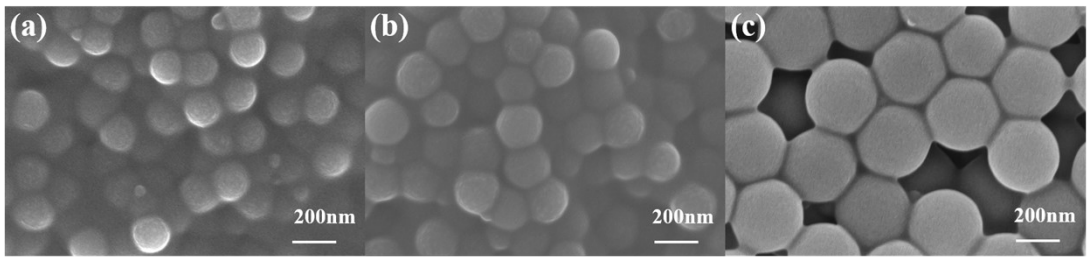


Fig. S2. The SEM images of PS (165 nm) (a), PS (200 nm) (b), PS (310 nm) (c)

As shown in Fig. S2a, the prepared PS spheres exhibit a well-defined spherical morphology with a narrow size distribution and an average diameter of approximately 165 nm. The particle surfaces are smooth, and the dispersion is uniform. Similarly, the PS spheres shown in Fig. S2b also display a uniform spherical shape with an average diameter of about 200 nm, indicating good monodispersity and minimal size variation. Furthermore, the PS spheres in Fig. S2c possess an average diameter of around 310 nm, and maintain an intact spherical morphology without noticeable aggregation. Overall, the three PS templates with different diameters present excellent monodispersity and structural uniformity, making them suitable as hard templates for constructing hollow $SiO_2$ layers with controllable cavity sizes, thus providing a reliable morphological basis for subsequent composite synthesis.

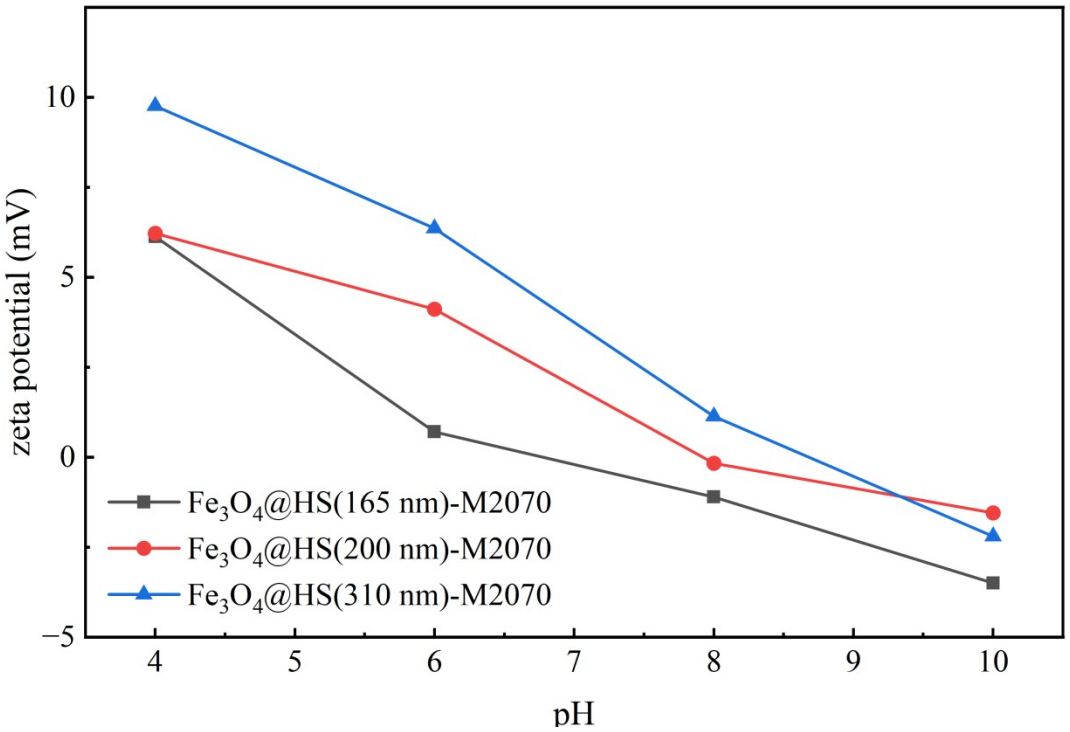


Fig. S3. Zeta potentials of $Fe_3O_4$@HS (165 nm)-M2070, $Fe_3O_4$@HS (200 nm)-M2070, and $Fe_3O_4$@HS (310 nm)-M2070 measured at different initial pH values.

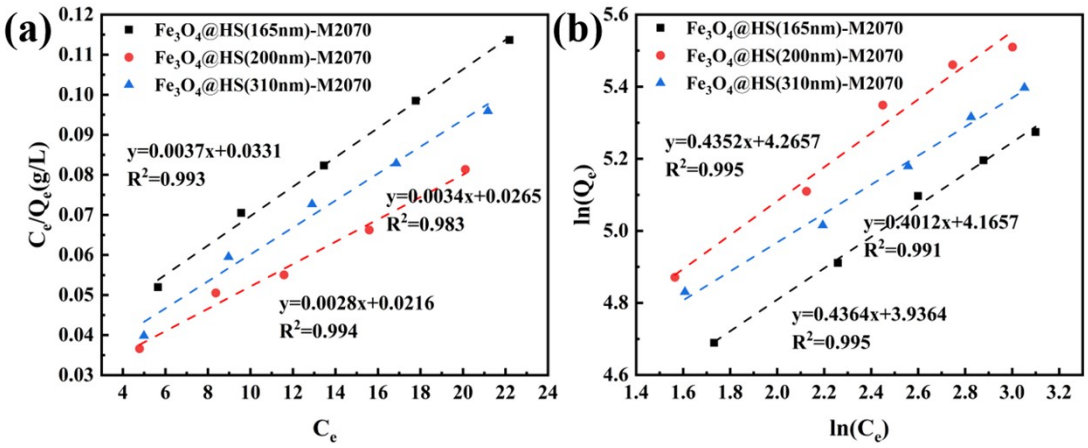


Fig. S4. The (a) Langmuir and (b) Freundlich model curves for $Fe_3O_4$@HS(165 nm, 200 nm, 310 nm)-M2070(pH=8, C0=20mg·$L^{-1}$, T=298K).

**Adsorption isotherm studies**

To further understand the relationship between the adsorbent and Pb(II), the experimental results are analyzed with the Langmuir and Freundlich isotherm models. The Langmuir model is applicable to monolayer adsorption, while the Freundlich adsorption model describes multilayer adsorption. These two adsorption isotherm models can be expressed by eq. (1) and (2) [76,77].

$$\frac{1}{Q_e} = \frac{1}{Q_m} + \frac{1}{K_L Q_m C_e} \quad (1)$$

$$L_n Q_e = L_n K_F + \frac{1}{n} L_n C_e \quad (2)$$

Where $Q_e$ (mg·$g^{-1}$) and $Q_m$ (mg·$g^{-1}$) represent the adsorption capacity at equilibrium and the maximum adsorption capacity of the adsorbent, respectively; $C_e$ (mg·$L^{-1}$) indicates the equilibrium concentration after adsorption; $K_L$(L·$mg^{-1}$) and $K_F$ (L·$mg^{-1}$) are the constants for the Langmuir and Freundlich models, respectively; and n is the empirical constant in the Freundlich model.

The linear fitting outcomes for both models are presented in Fig. S4a and b, with

the respective parameters provided in Table S1. Similar to the nonlinear fitting analysis, both models yield relatively high $R^2$ values, and slight differences between the Langmuir and Freundlich fittings again reflect the heterogeneous characteristics of the adsorbent surface. Pb(II) adsorption on all three materials can be adequately described by both isotherm models, further supporting the presence of multiple adsorption mechanisms, including heterogeneous and homogeneous interactions. Consistent with the nonlinear fitting analysis, the Freundlich model gives marginally higher $R^2$ values than the Langmuir model, suggesting a preference for heterogeneous multilayer adsorption. The 1/n values obtained from the Freundlich model are also below 1, indicating favorable Pb(II) adsorption onto $Fe_3O_4$@HS(165nm)-M2070, $Fe_3O_4$@HS(200nm)-M2070, and $Fe_3O_4$@HS(310nm)-M2070. Based on the Langmuir linear fitting, the estimated saturated adsorption capacities are 270.00, 357.14, and 294.00 $mg \cdot g^{-1}$ for Pb(II) on the three adsorbents, respectively. Although the pore dimensions differ between the 165 nm and 310 nm materials, their adsorption capacities remain comparable. This further confirms that comparable effective surface areas and accessible pore volumes after magnetic loading and functionalization may result in a similar density of active adsorption sites for Pb(II), which is consistent with the nonlinear fitting observations.

Table S1 The parameters of the adsorption isotherm model for the adsorption of Pb(II) by adsorbents

| PLs | Langmuir | | | Freundich | | |
|---|---|---|---|---|---|---|
| | $Q_m$ ($mg \cdot g^{-1}$) | $K_L$ ($L \cdot mg^{-1}$) | $R^2$ | $K_F$ ($L \cdot mg^{-1}$) | n | $R^2$ |

| | | | | | | |
|---|---|---|---|---|---|---|
| $Fe_3O_4$@HS(165nm)-M2070 | 270.00 | 0.112 | 0.993 | 51.23 | 2.291 | 0.995 |
| $Fe_3O_4$@HS(200nm)-M2070 | 357.14 | 0.130 | 0.994 | 71.21 | 2.298 | 0.995 |
| $Fe_3O_4$@HS(310nm)-M2070 | 294.00 | 0.128 | 0.983 | 64.43 | 2.493 | 0.991 |

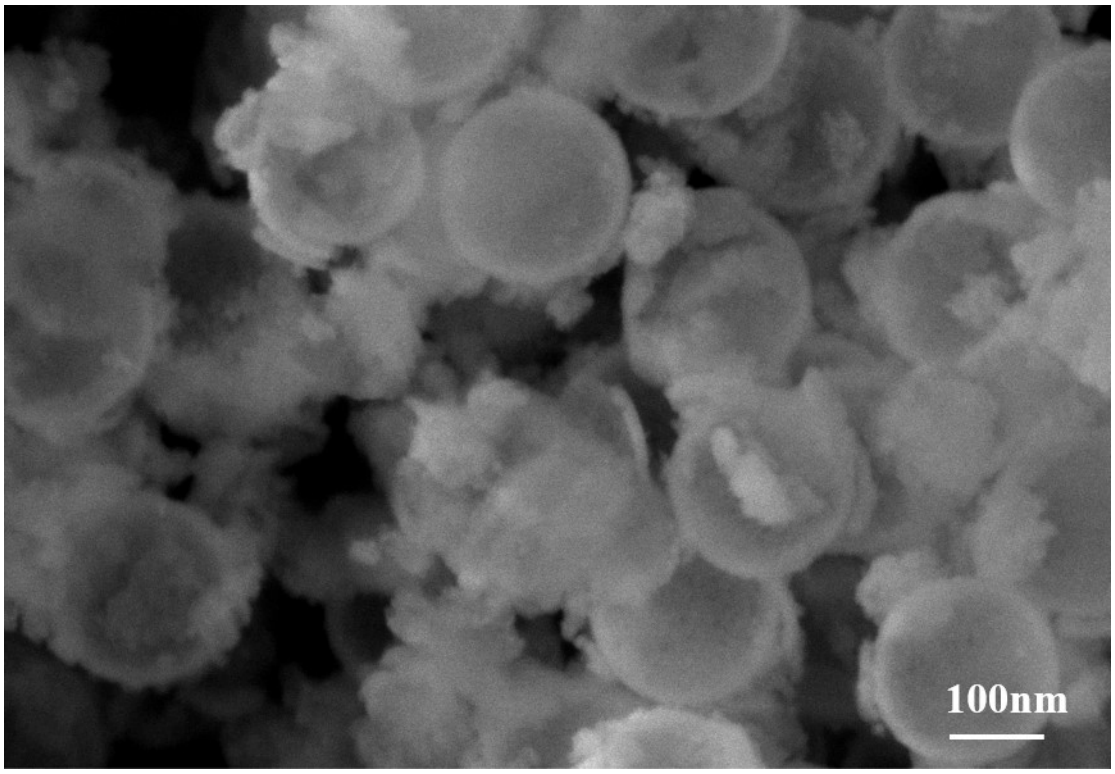


Fig. S5. SEM images of $Fe_3O_4$@HS-M2070 after 10 regeneration cycles.

Fig.S5 shows the SEM images of $Fe_3O_4$@HS-M2070 after 10 adsorption–desorption regeneration cycles. It can be seen that the overall morphology of the adsorbent remains relatively intact, and the hollow $SiO_2$ shells still retain their spherical structure. Only a small portion of the particles exhibit slight shell rupture or partial collapse, which may be attributed to the mechanical stress caused by repeated acid washing, rinsing, and magnetic separation processes. Nevertheless, most particles maintain good dispersion without significant aggregation or structural failure, indicating that the composite possesses excellent structural stability and regeneration durability. These results demonstrate that $Fe_3O_4$@HS-M2070 can sustain multiple regeneration cycles while maintaining its morphological integrity, ensuring its feasibility for long-term practical application.

Reference

75 Q. Zhang, J. Zhang, J. Shi and R. Yang, *Nanomaterials*, 2024, 14, 505, DOI: 10.3390/nano14060505.

76 Q. U. Ain, U. Rasheed, M. Yaseen, H. Zhang and Z. Tong, *Journal of Hazardous Materials*, 2020, **397**, 122758, DOI: 10.1016/j.jhazmat.2020.122758.

77 G. K. Rajahmundry, C. Garlapati, P. S. Kumar, R. S. Alwi and D.-V. N. Vo, *Chemosphere*, 2021, **276**, 130176, DOI: 10.1016/j.chemosphere.2021.130176.